Journal of Heat and Mass Transfer Research

Journal homepage: https://jhmtr.semnan.ac.ir

Semnan University

ISSN: 2383-3068

Research Article

Effect of Activation Energy on Magnetized Couple Stress Fluid over an Inclined Stretching Permeable Cylinder

Suman Sharma *, **Shalini Jain**

Department of Mathematics, University of Rajasthan, Jaipur, 302004, India

ARTICLE INFO

Article history:

Received: 2023-09-24

Revised: 2024-03-14

Accepted: 2024-03-31

Keywords:

Couple stress fluid;
Thermal radiation;
Non-Uniform heat source;
Soret effect;
Dufour effect;
Activation energy;
Non-Darcy medium;
Double stratification.

ABSTRACT

Activation energy is of considerable significance in diverse applications such as chemical kinetics, catalyst development, enzymes, semiconductors, and systems sensitive to temperature, such as chemical reactors and engines. The objective of this research is to investigate the influence of activation energy on a magnetized couple stress fluid over an inclined stretching permeable cylinder in a non-Darcy porous medium. The effects of cross-diffusion and stratified mixed convection are also considered in fluid model. The boundary layer equations, which describe the flow, have been converted into dimensionless form through suitable transformable variables. Subsequently, these transformed equations are solved using fourth order Runge-Kutta mechanism along with the shooting technique. The outcomes comprise visual depictions and comprehensive explanations demonstrating the influence of relevant variables on thermal, concentration, and velocity fields. Observations reveal that the concentration profile is directly influenced by the Forchheimer number and activation energy parameter, whereas both temperature and concentration fields decrease with elevated thermal and solutal stratification parameters. Additionally, numerical outcomes for the skin-friction coefficient, Nusselt number, and Sherwood number are presented in tabular form.

1. Introduction

Stokes [1] introduced couple stresses in viscous fluids, envisioning size-dependent effects that are absent in the polar case as the primary characteristic of couple stresses. Examples of fluids exhibiting couple stresses include lubricants with trace amounts of polymer additives, synthetic blood fluids, microfibers, and electro-rheological fluids. These materials find diverse industrial applications, such as in the extrusion of polymer fluids, the solidification of animal blood, and the study of liquid crystals. Rani et al. [2] investigated the flow of couple stress fluid around an infinite vertical cylinder, while Gajjela and Garvandha [3] examined the impact of cross diffusion and chemical reactions on couple stress flow through a stretching cylinder with convective boundary conditions.

Ibrahim and Gadisa [4] studied the behavior of a couple stress fluid around a stretching cylinder under conditions of double stratified mixed convection. Palaiah et al. [5] examined the impact of thermal radiation on magnetized couple stress fluid flowing over a vertical cylinder. Awais and Salahuddin [6] determined that the concentration profile of a couple stress fluid passing a paraboloid is enhanced with the increase in activation energy.

* **Corresponding author.**
E-mail address: s9549170542@gmail.com

Cite this article as:

Sharma, S. and Jain, S., 2025. Effect of Activation Energy on Magnetized Couple Stress Fluid over an Inclined Stretching Permeable Cylinder. *Journal of Heat and Mass Transfer Research*, 12(1), pp. 1-14.

https://doi.org/10.22075/JHMTR.2024.31879.1480

Activation energy holds crucial significance in various applications, including chemical kinetics, reactor cooling, emulsification of oil and water, catalyst and enzyme design, semiconductor processes, and temperature-sensitive systems such as chemical reactors and engines. Coined by Arrhenius [7], activation energy represents the minimum amount of energy required for chemical reactants to undergo a chemical reaction. Bestman [8] delved into boundary layer flow accompanied by activation energy and chemical reactions. Abbas et al. [9] observed that the concentration profile of Casson fluid over a stretching sheet increases with the activation energy parameter. Waqas et al. [10] examined the impact of activation energy and magnetic fields on couple stress nanofluid. Ibrahim and Negera [11] investigated the Williamson nanofluid model with activation energy effects around a stretching cylinder. Mustafa et al. [12] analyzed buoyancy-driven MHD nanofluid considering the influence of chemical reaction and activation energy on a vertical surface. Hamid et al. [13] explored Williamson nanofluid under the influence of activation energy. Awad et al. [14] studied activation energy and chemical reactions in unsteady rotating fluid flow. Jayarami Reddy and Suryanarayana Reddy [15] investigated the effects of heat generation and chemical reactions MHD boundary layer flow.

Darcy's law asserts that velocity is directly proportional to the pressure gradient, applicable primarily in laminar flow conditions with low velocity and porosity. However, Darcy's law becomes inadequate when inertial effects become significant. To address high-velocity flow, a non-Darcy term known as the Forchheimer drag parameter is introduced. Saeed et al. [16] explored the Darcy-Forchheimer flow of MHD hybrid nanofluid with heat transfer around a porous cylinder. Nagaraja et al. [17] investigated non-Newtonian flow influenced by a non-Darcy medium around a circular cylinder. Hayat et al. [18] analyzed the behavior of convective heat and mass transfer in flow around the inclined stretching cylinder. Ganesh et al. [19] examined Darcy-Forchheimer flow of MHD nanofluid with second-order slip conditions over a stretching sheet. Pal et al. [20] studied the impact of variable viscosity on the convective diffusion of species in a non-Darcy porous medium. Hayat et al. [21] examined Darcy-Forchheimer flow coupled with the Cattaneo-Christov model and variable thermal conductivity.

The application of heat transfer over a stretching cylinder has widespread applications in wire drawing, fire production, and hot rolling. Hayat et al. [22] analyzed the impact of thermal radiation and a non-uniform heat source on couple stress fluid in a thermally stratified medium over a stretching cylinder. Jain and Choudhary [23] studied the effects of suction and injection over a permeable horizontal cylinder in a porous medium. Khan et al. [24] developed the exact solutions for MHD flow of couple stress fluid. Jain and Parmar [25] analyzed Williamson fluid in the presence of a heat source.

Stratification of the medium involves the deposition or formation of layers due to temperature or concentration differences in different fluids. This phenomenon is characteristic of all fluid bodies surrounded by heated sidewalls. Parmar and Jain [26] studied heat transfer in Casson fluid flow through a cylinder. Rehman et al. [27] investigated double stratification for Williamson fluid flow in the presence of chemical reactions and mixed convection. Ramzan et al. [28] analyzed the thermal and solutal stratification effects on Jeffrey fluid around an inclined stretching cylinder with heat generation/absorption and thermal radiation. Sohut et al. [29] investigated the effect of double stratification along a stretching cylinder in the presence of chemical reactions. Rehman et al. [30] studied Eyring-Powell fluid flow in a dual stratified mixed convective medium with the effect of heat generation/absorption. Rashid et al. [31] studied the effects of nanoparticles shape on the heat transfer and nanofluid flow toward the stretching shrinking horizontal cylinder.

After observing the above-cited literature,

- It can be perceived that no research has been done to study the impact of activation energy on magnetized couple stress fluid over an inclined stretching permeable cylinder.
- The objective of this research is to analyse the impact of activation energy on magnetized couple stress fluid with cross-diffusion and double stratification.
- The boundary layer equations, which describe the flow, are converted into dimensionless form through suitable transformable variables. Subsequently, these transformed equations are solved using the fourth order Runge-Kutta mechanism along with shooting technique.
- Graphical representations are used to analyse results related to different parameters for velocity, temperature and concentration profiles. Additionally, numerical outcomes for the skin-friction coefficient, Nusselt number and Sherwood number are presented in tabular form.

2. Mathematical Formulation

We have considered two-dimensional, magneto double-stratified couple stress fluid flows past an inclined permeable stretching cylinder in a non-Darcy porous medium (See Fig. 1). The impacts of Activation energy, nonlinear thermal radiation, cross-diffusion and of non-uniform heat source are also taken. The x-axis is taken along the axis of cylinder and r-axis is normal to it. The cylinder is longitudinally stretching with velocity $U(x) = \frac{U_0}{L}x$, here U_0 is reference velocity and L is characteristic length. Inclination of the cylinder is denoted by α. A uniform magnetic field B_0 is also applied along r-direction. The temperature and concentration are maintained constant, symbolized by T_w and C_w respectively at surface and far from the boundary they are symbolized by T_∞ and C_∞ respectively.

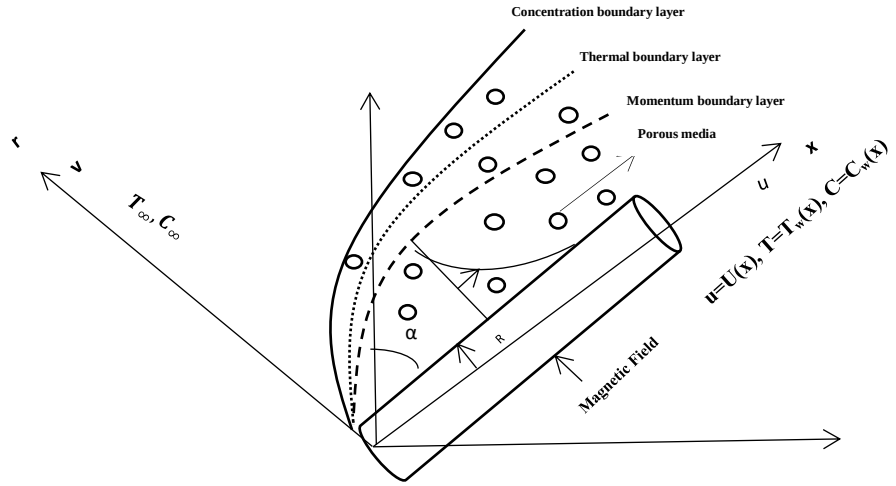

Fig. 1. Coordinate system and schematic diagram of the problem

Under above suppositions the equations of continuity, momentum, energy and concentration that govern the flow are written as:

Continuity equation

$$\frac{\partial(ru)}{\partial x} + \frac{\partial(rv)}{\partial r} = 0 \tag{1}$$

Momentum equation

$$\begin{aligned} u\frac{\partial u}{\partial x} + v\frac{\partial u}{\partial r} &= \upsilon\left(\frac{\partial^2 u}{\partial r^2} + \frac{1}{r}\frac{\partial u}{\partial r}\right) \\ &-\upsilon'\left(\frac{\partial^4 u}{\partial r^4} + \frac{2}{r}\frac{\partial^3 u}{\partial r^3} - \frac{1}{r^2}\frac{\partial^2 u}{\partial r^2} + \frac{1}{r^3}\frac{\partial u}{\partial r}\right) \\ &+(g\beta_1(T-T_\infty) + g\beta_2(T-T_\infty)^2)cos\alpha \\ &-\frac{\upsilon}{k'}u - F_0u^2 - \frac{\sigma B_0^2}{\rho}u \end{aligned} \tag{2}$$

Energy equation

$$\begin{aligned} &u\frac{\partial T}{\partial x} + v\frac{\partial T}{\partial r} = \\ &\frac{k_1}{\rho C_p}\left(\frac{1}{r}\frac{\partial T}{\partial r} + \frac{\partial^2 T}{\partial r^2}\right) + \frac{DK_T}{C_sC_P}\left(\frac{\partial^2 C}{\partial r^2} + \frac{1}{r}\frac{\partial C}{\partial r}\right) \\ &-\frac{1}{\rho C_p}\frac{1}{r}\frac{\partial(rq_r)}{\partial r} + q''\frac{1}{\rho C_p} \end{aligned} \tag{3}$$

Concentration equation

$$\begin{aligned} &u\frac{\partial C}{\partial x} + v\frac{\partial C}{\partial r} = \\ &D\left(\frac{1}{r}\frac{\partial C}{\partial r} + \frac{\partial^2 C}{\partial r^2}\right) + \frac{DK_T}{T_\infty}\left(\frac{\partial^2 T}{\partial r^2} + \frac{1}{r}\frac{\partial T}{\partial r}\right) \\ &-K_r^2(C-C_\infty)\left(\frac{T}{T_\infty}\right)^e \exp\left(\frac{-E_a}{k_2T}\right) \end{aligned} \tag{4}$$

in which T is the fluid temperature, C is the fluid concentration, g is gravity, β_1 is thermal expansion coefficient, β_2 is the coefficient of volumetric expansion, k' is the permeability of porous medium, σ is the electrical conductivity, $q_r = -\frac{16\sigma^* T_\infty^3}{3k^*}\frac{\partial T}{\partial r}$ is the radiative heat flux, σ^* is the Stefan-Boltzmann constant, k^* is the mean absorption coefficient, q'' is the rate of internal heat generations/absorption coefficient mentioned as:

$$q''' = \left(\frac{ku_w}{x\upsilon}\right)[X^*(T_w - T_\infty) + Y^*(T - T_\infty)] \tag{5}$$

where X^* and Y^* are space/time dependent heat source/ sink parameter (the case $X^* > 0$ and $Y^* > 0$ holds for internal heat generation, while $X^* < 0$ and $Y^* < 0$ for internal heat absorption), k is the thermal conductivity of the fluid, E_a is activation energy, κ_2 is the Boltzmann constant.

The appropriate boundary conditions as per formulation are prescribed as:

$$\text{At r=R,} \quad u = U(x) = \frac{U_0}{L}x,\ v = v_0,$$
$$T \to T_\infty(x) = T_0 + \frac{bx}{L},$$
$$C(x,r) = C_w(x) = C_0 + \frac{dx}{L}. \tag{6}$$
$$\text{as r}\to\infty, \quad u = 0,\ T \to T_\infty(x) = T_0 + \frac{cx}{L},$$
$$C \to C_\infty(x) = C_0 + \frac{ex}{L}.$$

here U_0 is reference velocity, L is characteristic length, and b, c, d and e are positive constant.

The stream function ψ that satisfies the continuity equation is define as

$$\text{u} = \frac{1}{\text{r}}\left(\frac{\partial\psi}{\partial\text{r}}\right) \text{ and v } = -\frac{1}{\text{r}}\left(\frac{\partial\psi}{\partial\text{x}}\right) \tag{7}$$

The dimensionless similarity transformations are:

$$u = \frac{U_0}{L}xf'(\eta), \qquad \eta = \frac{r^2 - R^2}{2R}\left(\frac{U_0}{\upsilon L}\right)^{\frac{1}{2}},$$
$$v = -\frac{R}{r}\left(\frac{U_0\upsilon}{L}\right)^{\frac{1}{2}}f(\eta), \quad \psi = \left(\frac{U_0\upsilon x^2}{L}\right)^{\frac{1}{2}}Rf(\eta), \tag{8}$$
$$\theta(\eta) = \frac{T - T_\infty}{T_w - T_0}, \qquad \phi(\eta) = \frac{C - C_\infty}{C_w - C_0}$$

Using these non-dimensional variables equations (1)-(4) are reduced into non-linear ordinary differential equations which are written as follows:

$$(1+2\gamma\eta)f''' + 2\gamma f'' + ff'' - (1+F)f'^2 - KRe[(1+2\gamma\eta)^2 f''''' + 8\gamma(1+2\gamma\eta)f'''' + 8\gamma^2 f'''] + (\theta + \gamma_1\theta^2)\lambda cos\alpha - (d+M)f' = 0 \tag{9}$$

$$Pr(f'\theta - f\theta') = \left(1 + \frac{4}{3}Rd\right)[2\gamma\theta' + (1+2\gamma\eta)\theta''] + PrD_f[2\gamma\phi' + (1+2\gamma\eta)\phi''] + [X(1-\delta_1)f' + Y\theta] \tag{10}$$

$$f'\phi - f\phi' = \frac{1}{Sc}(2\gamma\phi' + (1+2\gamma\eta)\phi'') + Sr(2\gamma\theta' + (1+2\gamma\eta)\theta'') - \sigma\phi(1+\zeta\theta)^e\, exp\left(\frac{-E}{1+\zeta\theta}\right) \tag{11}$$

Reduced boundary conditions are :

$$f(0) = -S, f'(0) = 1,$$
$$\theta(0) = 1 - \delta_1\,,$$
$$\phi(0) = 1 - \delta_2 \tag{12}$$
$$f' = f'' = f''' = \theta = \phi = 0 \quad as\ \eta \to \infty$$

Where, $F = xF_0$ Forchheimer number; $K = \frac{\upsilon'}{\upsilon R^2}$ Couple stress parameter; $Re = \frac{U_0R^2}{\upsilon L}$ Reynolds number; $d = \frac{\upsilon L}{U_0k'}$ porosity parameter; $\gamma = \left(\frac{\upsilon L}{U_0R^2}\right)^{\frac{1}{2}}$ curvature parameter; $\gamma_1 = \frac{\beta_2(T_w - T_0)}{\beta_1}$ nonlinear temperature convection coefficient; $\lambda = g(T_w - T_0)\beta_1\frac{L^2}{U_0^2 x}$ combined convection parameter; $M = \frac{\sigma B_0^2 L}{\rho U_0}$ magnetic field parameter; $Pr = \frac{\mu C_p}{K}$ Prandtl number; $f_w = v_0\sqrt{\frac{L}{U_0\nu}}$ suction/injection parameter $Rd = \frac{4\sigma_s T_\infty^3}{kk^*}$ thermal radiation parameter; $D_f = \frac{DK_T}{C_sC_p}\frac{d}{\upsilon b}$ Dufour number; X = space/time dependent heat source parameter; Y = space/time dependent heat sink parameter; $\delta_1 = \frac{c}{b}$ thermal stratification parameter; $Sc = \frac{\upsilon}{D}$ Schmidt number; $Sr = \frac{DK_T}{\upsilon T_\infty}\frac{b}{d}$ Soret number; $\sigma = K_r^2\frac{dx}{L}$ ratio rate parameter; $\zeta = \frac{T_w - T_0}{T_\infty}$ temperature difference parameter; $E = \frac{E_a}{K_2T_\infty}$ activation energy parameter; and the powers denote differentiation with respect to η.

The skin-friction coefficient C_f, Nusselt number Nu and Sherwood number Sh that characterize this study are given by:
Skin-friction coefficient

$$C_f = \frac{2\tau_w}{\rho U_w^2} \quad where \quad \tau_w\mu\left(\frac{\partial u}{\partial r}\right)_{r=R} \tag{13}$$

Nusselt number

$$Nu_x = \frac{-xq_w}{k(T_w - T_0)}\ where\ q_w = -k\left(\frac{\partial T}{\partial r}\right)_{r=R} \tag{14}$$

Sherwood number

$$Sh_x = \frac{-xj_w}{k(C_w - C_0)}\ where\ j_w = -D_B\left(\frac{\partial C}{\partial r}\right)_{r=R} \tag{15}$$

Using non-dimensional parameters equations (13-15) are written as:

$$C_f Re_x^{\frac{1}{2}} = -f''(0), \tag{16}$$

$$Nu_x Re_x^{\frac{-1}{2}} = -\theta'(0), \tag{17}$$

$$Sh_x Re_x^{-\frac{1}{2}} = -\phi'(0) \tag{18}$$

3. Solution of the Problem

The coupled ODEs (9)-(11) together with the transformed boundary conditions (12) are

unravelled by fourth order Runge-Kutta mechanism together with Shooting technique, using a MATLAB boundary value problem solver.

In the first step, the non-linear ODEs (9-11) are altered to first order differential equations.

Let

$f = f1,\ f' = f2,\ f'' = f3,\ f''' = f4,\ f'''' = f5,$
$\theta = f6,\ \theta' = f7,\ \phi = f8,\ \phi' = f9$

For these assumptions equations (9)-(11) will take the following form:

$$\begin{aligned} f^{(v)} = {} & K^{-1}Re^{-1}(1+2\gamma\eta)^{-2}[(1+2\gamma\eta)f4 \\ & + 2\gamma f3\ + f1f3 - (1+F)f2^2 \\ & -KRe\{8\gamma(1+2\gamma\eta)f5\ + 8\gamma^2 f4\} \\ & +\lambda cos\alpha(f6+\gamma_1 f6^2) - f2(M+d)] \end{aligned} \tag{19}$$

$$\theta'' = (1+2\gamma\eta)^{-1}\left(1+\frac{4}{3}Rd\right)^{-1} \times \begin{bmatrix} \Pr(f2f6 - f1f7) - 2\gamma\left(1+\frac{4}{3}Rd\right)f7 \\ -PrD_f\{2\gamma f9 + (1+2\gamma\eta)\phi''\} \\ -\{X(1-\delta_1)f1 + Yf6\} \end{bmatrix} \tag{20}$$

$$\begin{aligned} \phi'' = {} & (1+2\gamma\eta)^{-1}\Big[Sc\Big\{f2f8 - f1f9 - \\ & Sr(2\gamma f7 + (1+2\gamma\eta)\theta'') + \sigma f8(1+ \\ & \zeta f6)^e exp\left(\tfrac{E}{1+\zeta f6}\right)\Big\} - 2\gamma f9\Big] \end{aligned} \tag{21}$$

The reduced conditions (12) are:

$$\begin{aligned} & f1(0) = 0, \qquad f2(0) = 1, \\ & f6(0) = 1-\delta_1, \quad f8(0) = 1-\delta_2 \quad \text{and} \\ & f2(\infty) = f3(\infty) = f4(\infty) = f6(\infty) = \\ & f8(\infty) \to 0 \end{aligned} \tag{22}$$

We guess the values of f(3), f(7) and f(9), these are not given at initial conditions. Using step size 0.01 the process is continued, until we get the minimum error term.

4. Validation of the Study

Table 1 illustrates a comparison between the current findings and prior published studies conducted by Gajjela and Garvandha [3] and Hayat et al. [18]. The observed agreement between the present results and the earlier ones suggests a strong consistency. Furthermore, these findings serve to validate the accuracy of the current results.

Table 1. Comparison for the $f''(0)$ and $\theta'(0)$

	-f''(0)				-θ'(0)		
γ	[18]	[3]	Present	Pr	[18]	[3]	Present
0.0	1.6114	1.61145	1.61157	00.7	0.1902	0.19025	0.1905
00.05	1.6214	1.62142	1.62176	1	0.2035	0.20356	0.2042
00.1	1.6307	1.63071	1.63066	11.3	0.2127	0.21274	0.2133
00.15	1.6392	1.63915	1.6412	11.5	0.2174	0.21744	0.2282

5. Results and Discussion

To analyse the physical aspects of the considered problem, a comprehensive study have been done. The graphs for fluid velocity, concentration and temperature for the various values of involved parameters such as couple stress parameter, curvature parameter, Reynolds number, Forchheimer number, non-linear temperature convection coefficient, combined convection parameter, porosity parameter, thermal stratification parameter, Schmidt number and activation energy parameter are shown in Fig. 2 to 25. The numerical outcomes for local skin friction, Nusselt and Sherwood number are demonstrated graphically and in tabular form also (Table 1) with a good agreement with published literature. Figs. (2-4) sketched the impact of couple stress parameter on velocity, concentration and temperature fields respectively. Couple stress parameter K acts as a retardant agent because couple stress parameter increases the couple stress viscosity that causes denser fluid. It is perceived that the velocity profile fall off with increasing couple stress parameter K, temperature profile increases when K increases and concentration profile is increasing function of couple stress parameter.

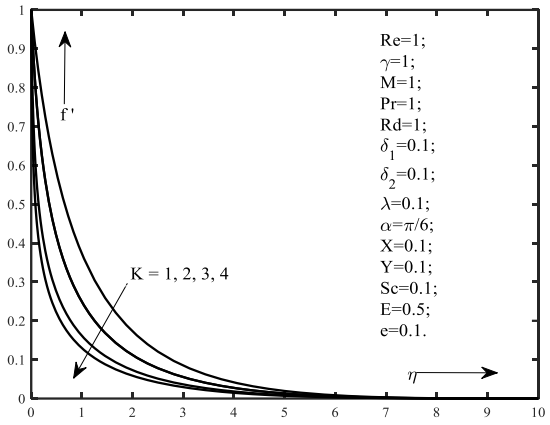

Fig. 2. Velocity distribution for K

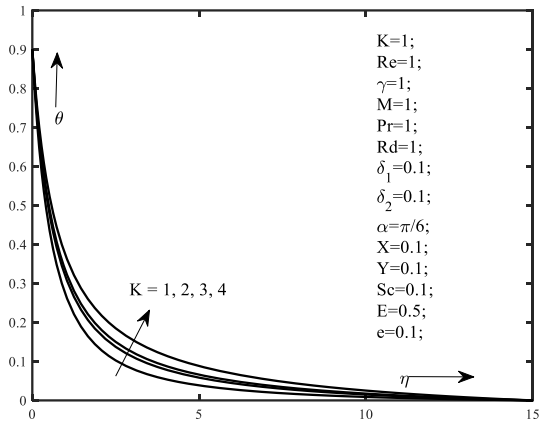

Fig. 3. Temperature distribution for K.

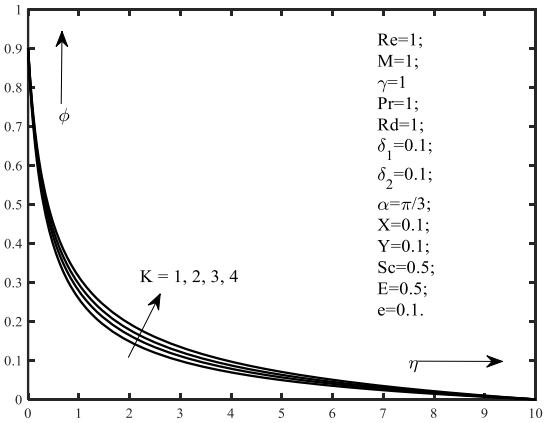

Fig. 4. Concentration distribution for K.

Figures (5-7) reveals the influence of curvature parameter. By raising the curvature parameter γ, the radius of cylinder reduces which cause to reduce contact area of fluid with cylinder. So the thickness of boundary layer reduces, thermal and concentration boundary layers become more thicker with curvature parameter γ. Hence as γ grow, the velocity field decreases near the surface of cylinder and enhances far away from surface and the temperature and concentration profiles increases. Figures (8-10) illustrates the impact of magnetic field on various fields. Magnetic field initiates a resistive force called Lorentz force. By increasing the value of magnetic field parameter M, the Lorentz force increases and the thickness of boundary layer reduces, therefore the velocity profiles fall off with an increase in the magnetic field. Thermal and concentration boundary layers become thicker with enhancing Lorentz force because it is a body retarding force that transverses the motion of the fluid and heat is evolved. It is shown in figure (9) and (10) that the profiles of temperature and concentrations are enhances with increasing magnetic field.

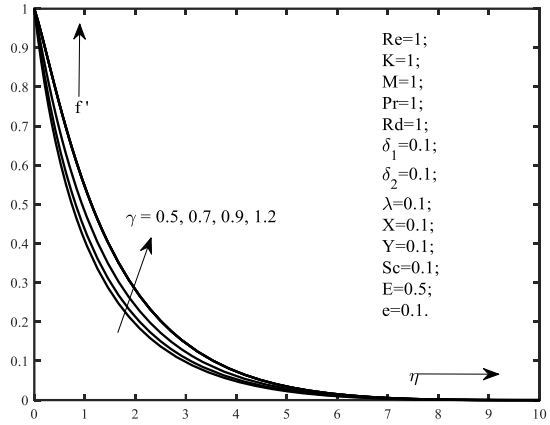

Fig. 5. Velocity distribution for γ.

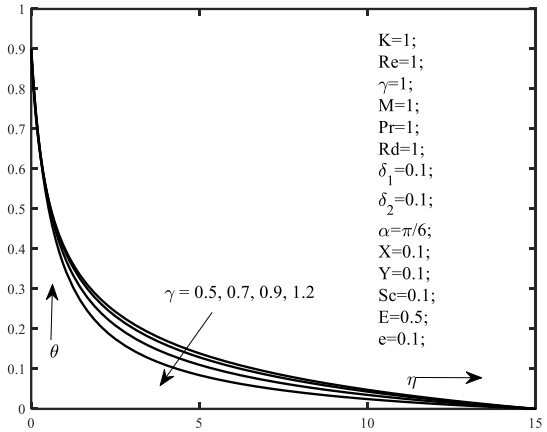

Fig. 6. Temperature distribution for γ.

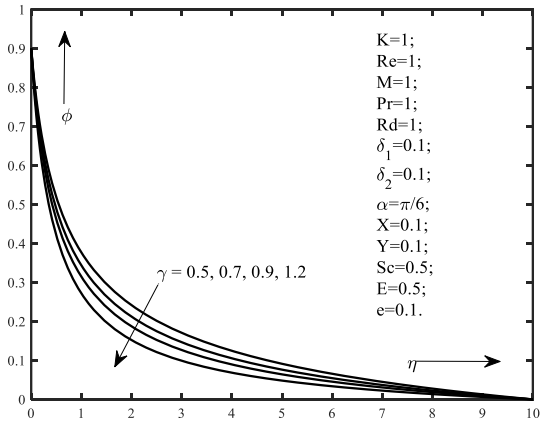

Fig. 7. Concentration distribution for γ.

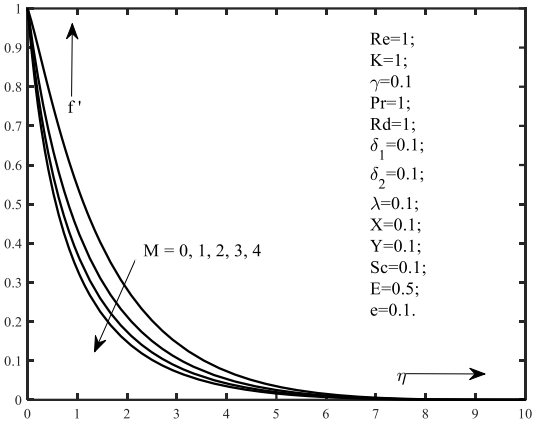

Fig. 8. Velocity distribution for M.

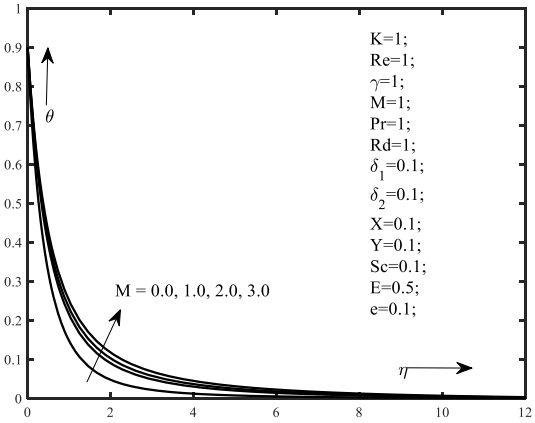

Fig. 9. Temperature distribution for M.

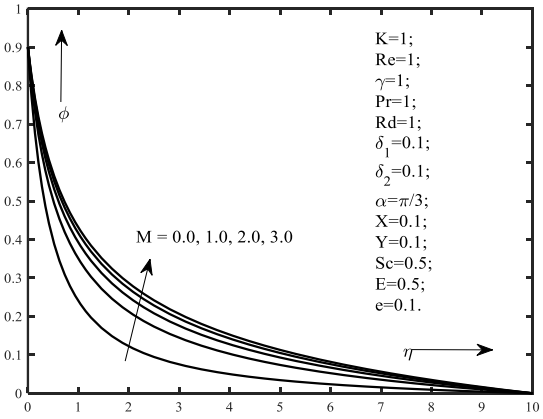

Fig. 10. Concentration distribution for M.

Figures (11-13) illustrate the impact of inclination angle. In Figure (11), it is observed that as the angle of inclination (α) increases, the velocity field decreases due to a decrease in gravitational force. When the angle of inclination rises, the effective gravitational force in the direction of flow reduces, leading to a weakening of the force propelling the fluid. As a result, the velocity field, which denotes the speed and direction of fluid flow, experiences a decline. Furthermore, the increased angle of inclination can result in a greater expanse of the cylinder's surface being subjected to fluid flow. This expanded surface area fosters increased interaction between the fluid and the cylinder, consequently enhancing the efficiency of heat and mass transfer. Hence, the thermal and concentration field Intensifies by enhancing inclination angle, depicted in figures (12-13).

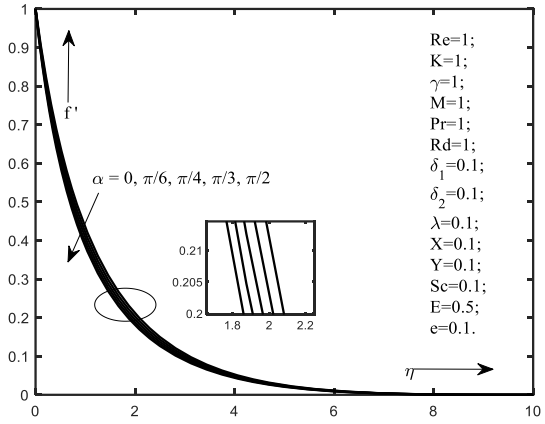

Fig. 11. Velocity distribution for α.

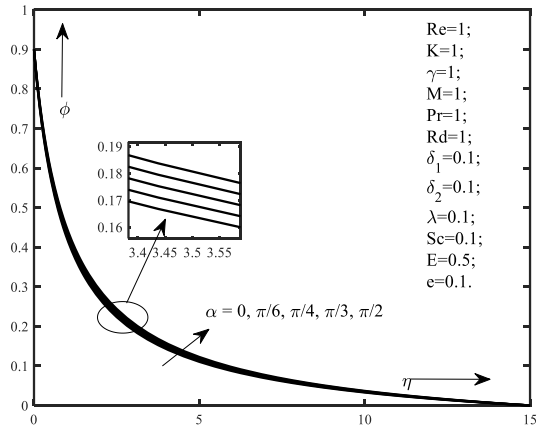

Fig. 12. Temperature distribution for α.

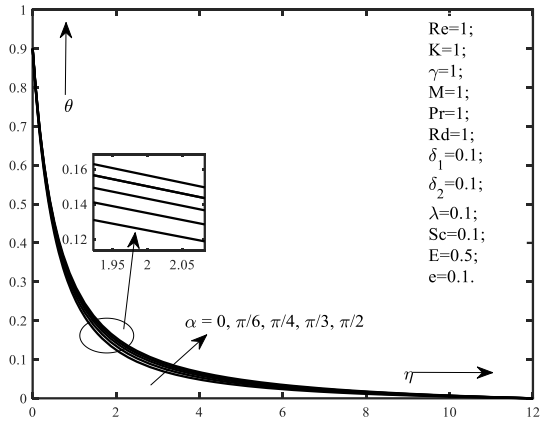

Fig. 13. Concentration distribution for α

Figure (14) anticipates effect of activation energy E on concentration profile. Concentration profile rises with increasing activation energy parameter because reaction rate constant decreases due to higher activation energy and low temperature, this increases the

concentration of solute. By increasing the Schmidt number Sc concentration profile decreases, it is shown in figure (15). Schmidt number is stated as the ratio of momentum diffusivity to mass diffusivity. Hence mass diffusivity reduces on increasing Schmidt number, which decreases the concentration profile.

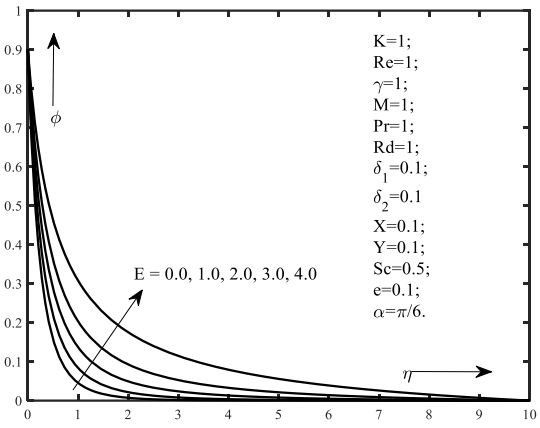

Fig. 14. Concentration distribution for E.

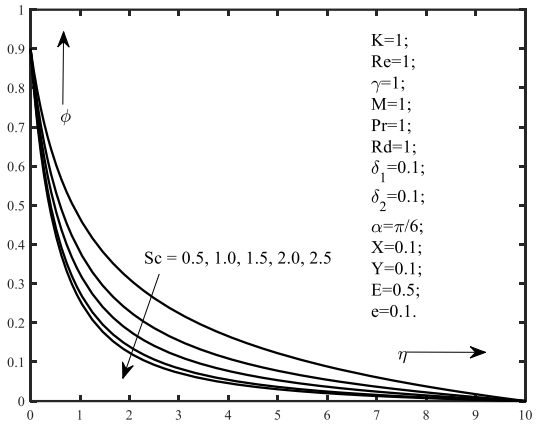

Fig. 15. Concentration distribution for Sc.

The effect of mixed convection parameter λ on velocity, thermal and concentration profiles is demonstrated in figures (16-18). As mixed convection grows, the buoyancy force dominates the viscous force that translates the flow from laminar to turbulent which hastens the flow of the fluid. Figure (16) display the mixed convection has the effect of enhancing the velocity profile. Thickness of thermal and concentration boundary layer reduces with enhancing buoyancy force. Hence the temperature and concentration profiles decreases with increasing mixed convection parameter λ.

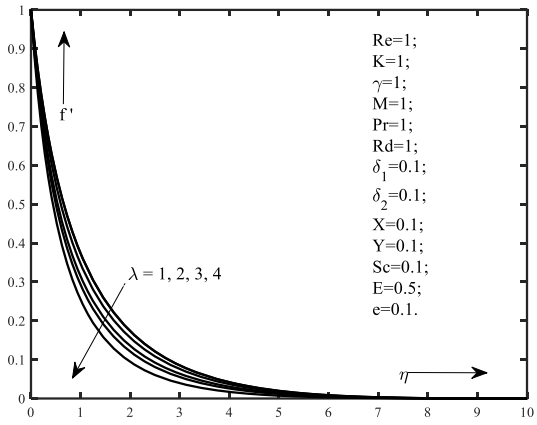

Fig. 16. Velocity distribution for λ.

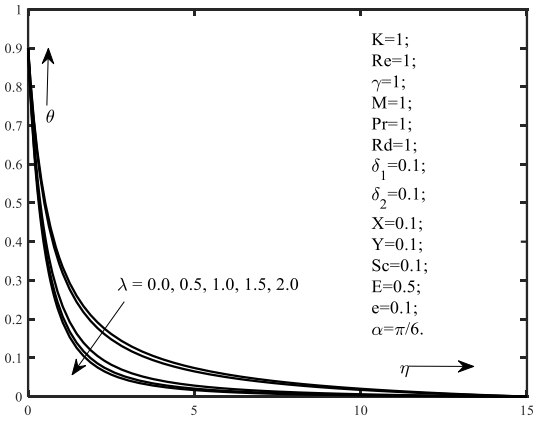

Fig. 17. Temperature distribution for λ.

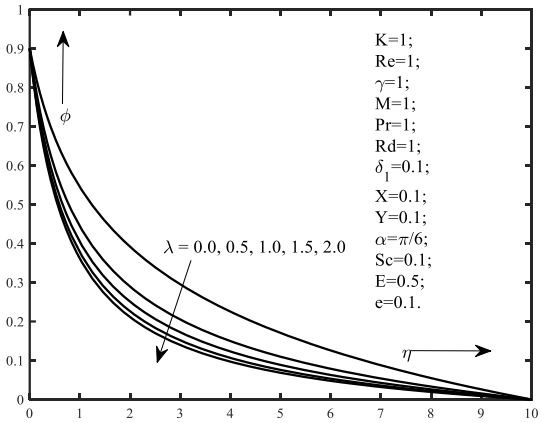

Fig. 18. Concentration distribution for λ.

Figures (19-20) represents that the temperature and concentration profile decreases with thermal stratification $\delta 1$ and solutant stratification parameter $\delta 2$ because when stratification increase then the convective potential between the fluid and surface of cylinder declines.

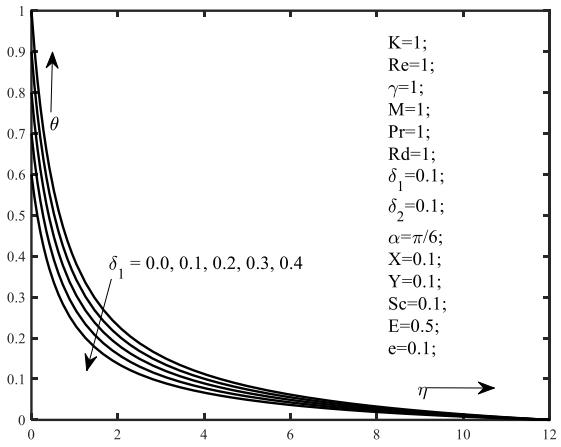

Fig. 19. Temperature distribution for δ_1.

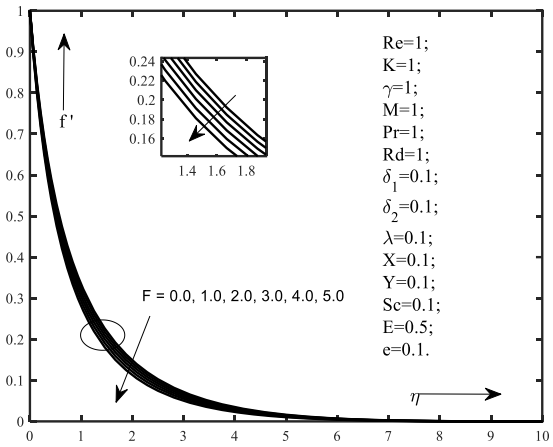

Fig. 21. Velocity distribution for F.

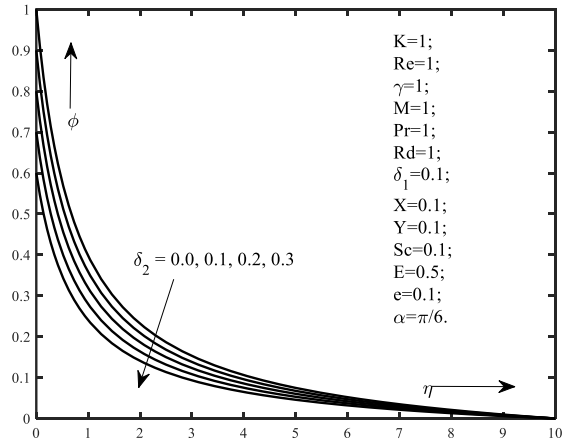

Fig. 20. Concentration distribution for δ_2.

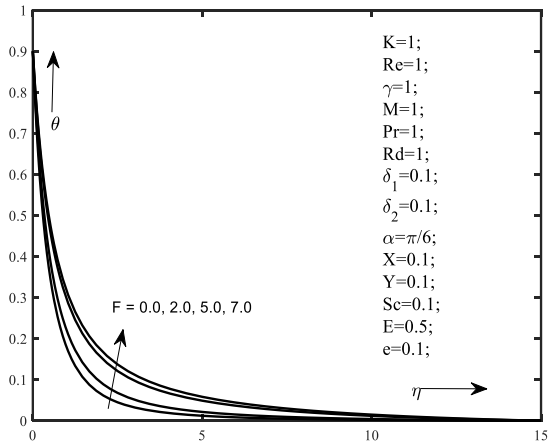

Fig. 22. Temperature distribution for F.

In figures (21-23) it is observed that the velocity profile decreases, temperature and concentration increases with an increasing Forchheimer number F. In the realm of permeability, the Forchheimer number delineates the balance between inertial and viscous forces governing fluid flow within porous materials, offering insight into the complex dynamics of fluid behavior. A high Forchheimer number signifies the dominance of inertial effects. Higher value of inertial coefficient produces resistance in the flow path. Thus, the thickness of velocity boundary layer reduces, thermal and concentration boundary layers enhances with Darcy Forchheimer number.

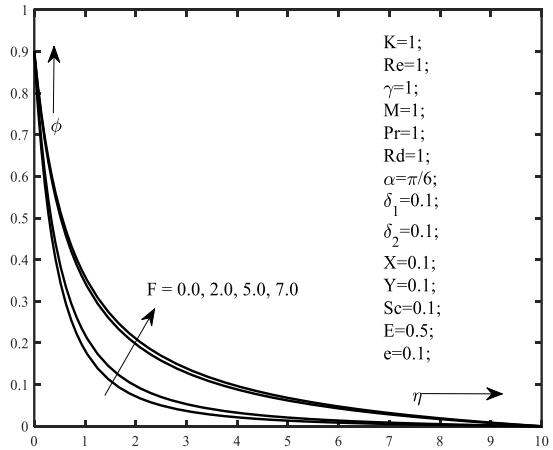

Fig. 23. Concentration distribution for F.

Figures (24-26) depicts the effect of Soret and Dufour number on boundary profiles. The values of Soret and Dufour are taken in such way that their product is constant. When Sr is raised, there will be a higher thermal diffusion. It is observed in figure (24) that the velocity enhances for high Dufour number and temperature and concentration profiles (25-26) decreases for high dufour number.

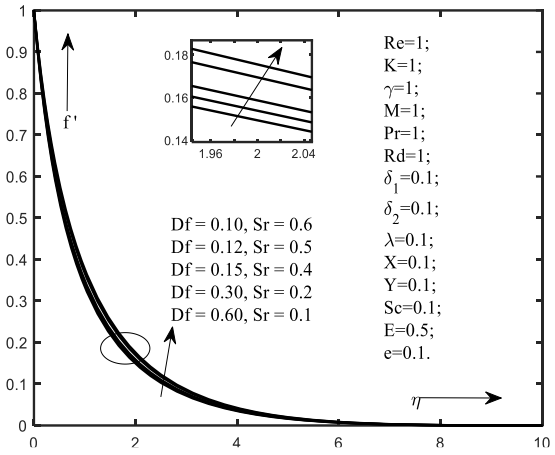

Fig. 24. Velocity distribution for Sr and Du.

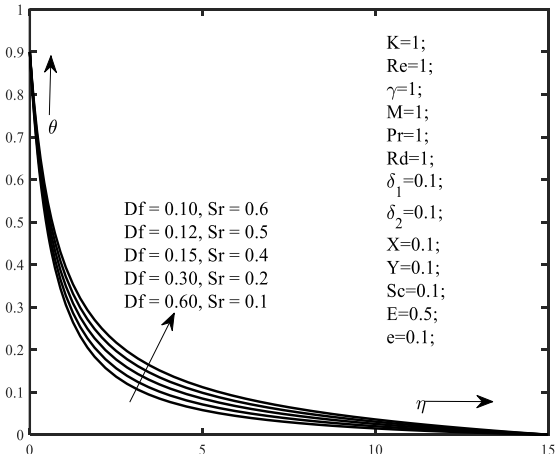

Fig. 25. Temperature distribution for Sr and Du.

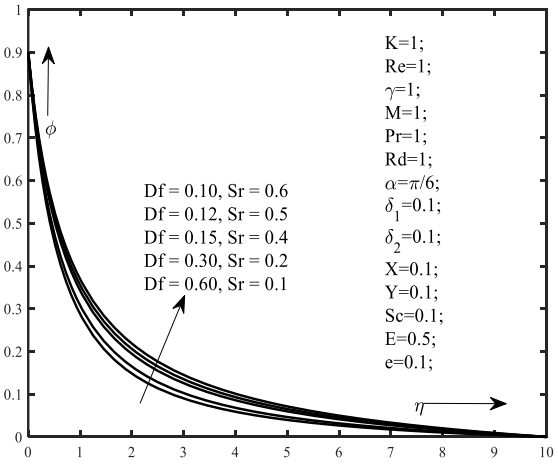

Fig. 26. Concentration distribution for Sr and Du.

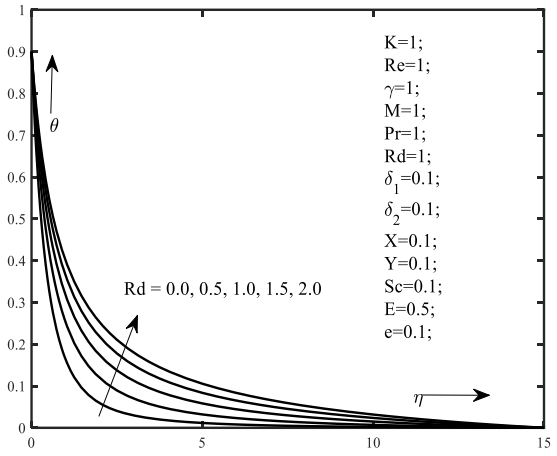

Fig. 27. Temperature distribution for Rd.

Figure (27) shows the effect of thermal radiation parameter on thermal profile. An increase in the radiation parameter Rd means a decrease in the Rosseland radiation absorptivity κ^* and this increases the divergence of radiative heat flux. Hence it is observed that the temperature increases as thermal radiation parameter upsurge. Figure (28) displays declined in temperature profile when the value of prandtl number (Pr) rise. Higher prandtl number has low thermal conductivity which results in heat conduction and thus the temperature profile decreases with higher Prandtl number.

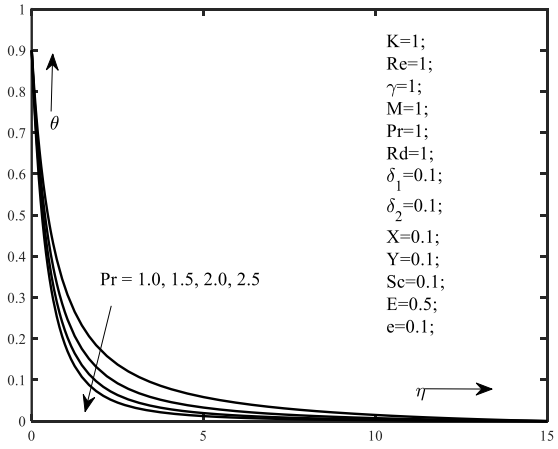

Fig. 28. Temperature distribution for Pr

Numerical results of skin friction coefficient $f''(0)$, Nusselt number $\theta'(0)$ and Sherwood number $\phi'(0)$ for various physical parameters are presented in 2.

6. Conclusions

In this paper we studied the impact of activation energy on magnetized couple stress fluid over an inclined stretching permeable cylinder in a non-Darcy porous medium. The effects of cross-diffusion and stratified mixed

convection are also considered in fluid model. The governing PDEs are remoulded into dimensionless nonlinear ODEs by using appropriate similarity transformations and then unravelled by fourth order Runge-Kutta mechanism along with shooting technique. The key results of this study are as follows :

- Upsurging values of couple stress parameter and magnetic parameters depreciate the velocity field, while improves the temperature and concentration field.
- The curvature parameter has enhancing impact on velocity profile, while it reduces the temperature and concentration fields.
- Activation energy has portionate impact on concentration field, although Schmidt number has an adverse effect.
- The prevailing values of Convection parameter boost the velocity field, but have reverse effect on temperature and concentration fields.
- Temperature and concentration fields depreciate with higher thermal and solutal stratification parameter respectively.
- Velocity, temperature and concentration fields are strengthened by increasing the values of Forchheimer number.
- Temperature field is an increasing function of thermal radiation parameter and decreasing function of Prandtl number.

Nomenclature

$C_\infty(x)$ Variable ambient concentration $(Kmol/m^3)$

$C_w\ (x)$ The prescribed surface concentration $(Kmol/m^3)$

D_f Dufour number

E Activation energy parameter

C_0 Reference concentration $(Kmol/m^3)$

F Forchheimer number

M Magnetic field parameter

T_0 Reference temperature (K)

U_0 Free stream velocity (ms^{-1})

Re Reynolds number

Pr Prandtl number

Rd Thermal radiation parameter

Sc Schmidt number

Sr Soret number

g Gravitational acceleration (ms^{-2})

k Thermal conductivity $(Wm^{-1}K^{-1})$

k' Permeability of porous medium (m^2)

c_p Specific heat at constant pressure $(Jkg^{-1}K^{-1})$

K Couple stress parameter

L Reference length (m)

B_0 Uniform magnetic field (Wbm^{-2})

X^* Space/time dependent heat source parameter

Y^* Space/time dependent heat sink parameter

$T_\infty\ (x)$ Variable ambient temperature (K)

$T_w\ (x)$ The prescribed surface temperature (K)

$U(x)$ Stretching velocity (ms^{-1})

d Porosity parameter

D Mass diffusivity (m^2s^{-1})

E_a Activation energy $(kJmol^{-1})$

k_r Chemical reaction rate constant

Greek symbols

δ_1 Thermal stratification parameter

α Inclination of the cylinder

γ Curvature parameter

ζ Temperature difference parameter

λ Combined convection parameter

σ Electrical conductivity $(m^{-1}Ohm^{-1})$

ν Kinematic viscosity (m^2s)

ν' Couple stress viscosity ($m^2 s$)

γ_1 Nonlinear temperature convection coefficient

Funding Statement

This research has been conducted with financial assistance from UGC, India, in the form of a senior research fellowship under UGC-Ref. No.: 1294/ (CSIR-UGC NET JUNE 2019 granted to Suman Sharma.

Conflicts of Interest

The author declares that there is no conflict of interest regarding the publication of this article.

References

[1] Stokes, V. K., 1966. Couple stresses in fluids. Phys. Fluids, 9(9), pp. 1709–1715. doi: 10.1063/1.1761925.

[2] Rani, H.P., G. J. Reddy, G. J., and Kim C. N., 2011. Numerical analysis of couple stress fluid past an infinite vertical cylinder. *Eng. Appl. Comput. Fluid Mech.,* 5(2), pp. 159–169. doi: 10.1080/19942060.2011.11015360.

[3] Gajjela, N. and Garvandha, M., 2020. The influence of magnetized couple stress heat, and mass transfer flow in a stretching cylinder with convective boundary condition, cross-diffusion, and chemical reaction. *Therm. Sci. Eng. Prog.*, 18, pp. 100517. doi: 10.1016/j.tsep.2020.100517.

[4] Ibrahim, W. and Gadisa, G., 2020. Double Stratified Mixed Convective Flow of Couple Stress Nanofluid past Inclined Stretching Cylinder Using Cattaneo-Christov Heat and Mass Flux Model. *Advances in Mathematical Physics, 2020(1), p. 4890152.* doi: 10.1155/2020/4890152.

[5] Palaiah, S. S., Basha, H., and Reddy G. J., 2021. Magnetized couple stress fluid flow past a vertical cylinder under thermal radiation and viscous dissipation effects. *Nonlinear Eng.*, 10(1), pp. 343–362. doi: 10.1515/nleng-2021-0027.

[6] Awais, M. and Salahuddin, T., 2023. Natural convection with variable fluid properties of couple stress fluid with Cattaneo-Christov model and enthalpy process. *Heliyon,* 9(8), pp. 18546. doi: 10.1016/j.heliyon.2023.e18546.

[7] Arrhenius, S., 1889. Über die Dissociationswärme und den Einfluss der Temperatur auf den Dissociationsgrad der Elektrolyte / About the heat of dissociation and the influence of temperature on the degree of dissociation of the electrolytes (in German). *Zeitschrift für Phys. Chemie*.

[8] Bestman, A. R., 1990. Natural convection boundary layer with suction and mass transfer in a porous medium. *Int. J. Energy Res.*, 14(4), pp. 389–396. doi: 10.1002/er.4440140403.

[9] Abbas, Z., Sheikh, M. and Motsa, S. S., 2016. Numerical solution of binary chemical reaction on stagnation point flow of Casson fluid over a stretching/shrinking sheet with thermal radiation. *Energy*, 95, pp. 12–20. doi: 10.1016/j.energy.2015.11.039.

[10] Waqas, H., Wakif, A., Al-Mdallal, Q., Zaydan, M., Farooq, U. and Hussain, M., 2022. Significance of magnetic field and activation energy on the features of stratified mixed radiative-convective couple-stress nanofluid flows with motile microorganisms. *Alexandria Eng. J.*, 61(2), pp. 1425–1436. doi: 10.1016/j.aej.2021.06.047.

[11] Ibrahim, W., and Negera, M. 2020. The Investigation of MHD Williamson Nanofluid over Stretching Cylinder with the Effect of Activation Energy. *Adv. Math. Phys.* doi: 10.1155/2020/9523630.

[12] Mustafa, M., Khan, J.A., Hayat, T., and Alsaedi, A., 2017. Buoyancy effects on the MHD nanofluid flow past a vertical surface with chemical reaction and activation energy. *Int. J. Heat Mass Transf.*, 108, pp. 1340–1346. doi: 10.1016/j.ijheatmasstransfer.2017.01.029.

[13] Hamid, A., Khan, M. and Khan, U., 2018. Thermal radiation effects on Williamson fluid flow due to an

expanding/contracting cylinder with nanomaterials: Dual solutions. *Phys. Lett. Sect. A Gen. At. Solid State Phys.*, 382(30), pp. 1982–1991. doi: 10.1016/j.physleta.2018.04.057.

[14] Awad, F. G., Motsa, S. and Khumalo, M., 2014. Heat and mass transfer in unsteady rotating fluid flow with binary chemical reaction and activation energy. *PLoS One*, 9(9). doi: 10.1371/journal.pone.0107622.

[15] Reddy, K. J. and Reddy, M. S., 2013. Effects Of Chemical Reaction And Heat Generation On MHD Boundary Layer Flow Of A Moving Vertical Plate With Suction And Dissipation. *i-manager's J. Futur. Eng. Technol.*, 8(4), pp. 30–40. doi: 10.26634/jfet.8.4.2359.

[16] Saeed, A., Kumam, P., Gul, T., Alghamdi, W., Kumam, W. and Khan, A., 2021. Darcy–Forchheimer couple stress hybrid nanofluids flow with variable fluid properties. *Sci. Rep.*, 11(1), pp. 1–13. doi: 10.1038/s41598-021-98891-z.

[17] Nagaraja, L., Reddy, M. S. N., 2017. Heat Transfer in a Non-Newtonian Fluid Past a Horizontal Circular Cylinder in Non-Darcy Porous Medium with Suction\Injection Effects. *Indian J. Sci. Technol.*, 10(32), pp. 1–7. doi: 10.17485/ijst/2017/v10i32/104601.

[18] Hayat, T., Saeed, Y., Asad, S. and Alsaedi, A., 2016. Convective heat and mass transfer in flow by an inclined stretching cylinder. *J. Mol. Liq.*, 220, pp. 573–580. doi: 10.1016/j.molliq.2016.03.047.

[19] Ganesh, N. V., Abdul Hakeem, A. K. and Ganga, B., 2018. Darcy–Forchheimer flow of hydromagnetic nanofluid over a stretching/shrinking sheet in a thermally stratified porous medium with second order slip, viscous and Ohmic dissipations effects. *Ain Shams Eng. J.*, 9(4), pp. 939–951. doi: 10.1016/j.asej.2016.04.019.

[20] Pal, D. and Mondal, H., 2010. Effect of variable viscosity on MHD non-Darcy mixed convective heat transfer over a stretching sheet embedded in a porous medium with non-uniform heat source/sink, *Commun. Nonlinear Sci. Numer. Simul.*, 15(6), pp. 1553–1564. doi: 10.1016/j.cnsns.2009.07.002.

[21] Hayat T., Asad, S. and Alsaedi, A., 2017. Non-uniform heat source/sink and thermal radiation effects on the stretched flow of cylinder in a thermally stratified medium. *J. Appl. Fluid Mech.*, 10(3), pp. 915–924. doi: 10.18869/acadpub.jafm.73.240.24008.

[22] Hayat, T., Asad, S., Alsaedi, A. and Alsaadi, F.E., 2015. Radiative flow of jeffrey fluid through a convectively heated stretching cylinder. *J. Mech.*, 31(11), pp. 69–78. doi: 10.1017/jmech.2014.49.

[23] Jain, S., and Choudhary, R., 2017. Soret and Dufour effects on MHD fluid flow due to moving permeable cylinder with radiation. *Glob. Stoch. Anal*, 4, pp. 75–84.

[24] Khan, N. A., Khan, H. and Ali, S. A., 2016. Exact solutions for MHD flow of couple stress fluid with heat transfer. *J. Egypt. Math. Soc.*, 24(1), pp. 125–129. doi: 10.1016/j.joems.2014.10.003.

[25] Jain, S. and Parmar, A., 2018. Radiation Effect on MHD Williamson Fluid Flow over Stretching Cylinder Through Porous Medium with Heat Source. *Lect. Notes Mech. Eng.*, 0, pp. 61–78. doi: 10.1007/978-981-10-5329-0_5.

[26] Bilal, S., Rehman, K. U. and Malik, M. Y., 2017. Numerical investigation of thermally stratified Williamson fluid flow over a cylindrical surface via Keller box method. *Results Phys.*, 7, pp. 690–696. doi: 10.1016/j.rinp.2017.01.032.

[27] Rehman, K. U., Khan, A. A., Malik, M. Y. and Ali, U., 2017. Mutual effects of stratification and mixed convection on Williamson fluid flow under stagnation region towards an inclined cylindrical surface. *MethodsX*, 4, pp. 429–444. doi: 10.1016/j.mex.2017.10.007.

[28] Ramzan, M., Bilal, M. and Chung, J. D., 2017. Effects of thermal and solutal stratification on jeffrey magneto-nanofluid along an inclined stretching cylinder with thermal radiation and heat generation/absorption. *Int. J. Mech. Sci.*, 131–132, pp. 317–324. doi: 10.1016/j.ijmecsci.2017.07.012.

[29] Mohd Sohut, N. F. H., Abd Aziz, A. S. and Ali, Z. M., 2017. Double stratification effects on boundary layer over a stretching cylinder with chemical reaction and heat generation. *J. Phys. Conf. Ser.*, 890(1). doi: 10.1088/1742-6596/890/1/012019.

[30] Rehman, A. and Nadeem, S., 2013. Heat Transfer Analysis of the Boundary Layer Flow over a Vertical Exponentially Stretching Cylinder. *Glob. J. Sci. Front. Res. Math. Decis. Sci.*, 13(11).

[31] Rashid, U., Liang, H. Ahmad, H., Abbas, M., Iqbal, A., and Hamed, S., 2021. Results in Physics Study of (Ag and TiO2)/ water nanoparticles shape effect on heat transfer and hybrid nanofluid flow toward stretching shrinking horizontal cylinder. *Results Phys.*, 21. doi: 10.1016/j.rinp.2020.103812.